arXiv:1403.4792v1 [cond-mat.mes-hall] 19 Mar 2014

Coupling graphene mechanical resonators to superconducting microwave cavities

P. Weber*, J. Güttinger*†, I. Tsioutsios, D. E. Chang, A. Bachtold

ICFO-Institut de Ciencies Fotoniques,Mediterranean Technology Park, 08860 Castelldefels (Barcelona), Spain

Abstract

Graphene is an attractive material for nanomechanical devices because it allows for exceptional properties, such as high frequencies and quality factors, and low mass. An outstanding challenge, however, has been to obtain large coupling between the motion and external systems for efficient readout and manipulation. Here, we report on a novel approach, in which we capacitively couple a high-Q graphene mechanical resonator ($Q \sim 10^5$) to a superconducting microwave cavity. The initial devices exhibit a large single-photon coupling of ~ 10 Hz. Remarkably, the large capacitive coupling also enables strong tuning of the graphene equilibrium position, renormalization of the single-photon coupling, and softening of the mechanical resonance frequency. We also observe a Duffing nonlinearity whose sign and magnitude can be controlled via a constant voltage applied to the graphene. With realistic improvements, it should be possible to enter the regime of quantum optomechanics.

[∗] These authors contributed equally to this work.
[†] Corresponding author. E-mail johannes.guettinger@icfo.es.

Mechanical resonators based on indivitual nanotubes and graphene flakes have outstanding properties. Their mass is ultra-low, their quality factor can be remarkably high, the resonance frequency is widely tunable, and their equilibrium position can be varied by a large amount. As a result, the resonators are sensors of mass [1, 2] and force [3–5] with unprecedented sensitivities, and they can be employed as parametric amplifiers [6] and as tunable oscillators [6–8]. All these scientific applications are accomplished in the classical regime.

Reaching the quantum regime with mechanical resonators has attracted considerable interest [9, 10]. Thus far, three groups have been successful in this quest by demonstrating that the number of vibrational quanta can be lowered below one [11–13]. These three groups were using different resonators, namely, a piezoelectric resonator, a superconducting resonator, and an opto-mechanical crystal. There is now an intense effort from the community to develop new types of opto-mechanical and electro-mechanical devices, the goal being to explore new scientific and technological applications when these devices will enter the quantum regime. This includes levitating particles [14, 15], optically trapped cantilevers [16], and heavy pillars [17] to test the foundations of quantum mechanics; metal coated silicon nitride membranes to coherently convert radiofrequency photons to visible photons [18, 19]; microdisks and nanopillars to boost the single-photon coupling and to enter the ultra strong coupling regime [20, 21]. In this context, the unique properties of nanotube and graphene resonators are very interesting.

Although nanotube and graphene have exceptional properties, an outstanding challenge in approaching the quantum regime has been the development of efficient coupling to external elements, which would enable motional readout and manipulation. For example, while graphene has been coupled to an optical cavity [22], the 2.3% optical absorption of graphene makes it extremely challenging to reach the quantum regime, due to heating of the graphene and quenching of the optical cavity finesse. Here, we employ a different strategy, which is to couple the mechanical resonator capacitatively to a superconducting cavity [12, 23–27]. This is a promising approach with graphene resonators, because the two-dimensional shape of graphene is ideal for large capacitive coupling.

In this work we report on the integration of a circular graphene resonator with a superconducting microwave cavity. We use a transfer technique to precisely position a high-quality exfoliated graphene flake with respect to a predefined superconducting cavity. We develop

a reliable method to reduce the separation between the graphene membrane and the cavity by tightly clamping the graphene sheet inbetween a support electrode and a cross-linked Polymethyl methacrylate (PMMA) structure. This technique allows us to improve the mechanical stability and to achieve high mechanical quality factors. By pumping the cavity on a motional sideband, we are able to sensitively readout the graphene motion. Importantly, by applying a constant voltage $V_{\rm g}^{\rm DC}$ to the graphene, the properties of the optomechanical device can be dramatically tuned. Namely, large static forces can be produced, allowing to tune the steady-state displacement, the mechanical resonance frequency, the optomechanical coupling, and the mechanical nonlinearities.

Our device (see Fig. 1) consists of a superconducting microwave cavity, modeled as a LC-circuit with angular frequency $\omega_c = 1/\sqrt{LC_{tot}}$. The total capacitance $C_{\rm tot} = C + C_{\rm ext} + C_{\rm m}(z)$ effectively consists of a cavity capacitance C, a contribution C_{ext} from the external feedline, and importantly, a contribution $C_{\rm m}(z)$ that depends on the graphene position z, which arises from the graphene acting as a moving capacitor plate. A small displacement z therefore produces a shift in $\omega_{\rm c}$ quantified by the optomechanical coupling $G_0 = \frac{\partial \omega_{\rm c}}{\partial z}$. As a result, the interaction between the mechanical resonator and the superconducting cavity can be described by the Hamiltonian $H_{\rm int} = \hbar G_0 n_{\rm p} z$ [12] with $n_{\rm p}$ the number of pump photons in the cavity. The characteristic coupling at the level of the zero-point motion $z_{\rm zp} = \sqrt{\hbar/2m_{\rm eff}\omega_m}$ is given by the so-called single-photon coupling $g_0 = G_0 z_{\rm zp}$, with $m_{\rm eff}$ the effective mass and $\omega_{\rm m}/2\pi$ the resonance frequency of the mechanical mode of interest. Central to this work is *(i)* that the low mass of graphene boosts $z_{\rm zp}$ and thus g_0, and *(ii)* that $C_{\rm m}$ and g_0 can be tuned electrostatically with $V_{\rm g}^{\rm DC}$.

We start with engineering considerations in order to maximize the coupling g_0. When describing C_m by a plate capacitor and noting that $C \gg C_{\rm ext} \gg C_{\rm m}(z)$ in our device, we have that $g_0 \approx \frac{\omega_{\rm c}}{2C}\frac{\partial C_{\rm m}(z)}{\partial z} z_{\rm zp} \propto \sqrt{\frac{A}{\omega_{\rm m}}}\frac{\omega_{\rm c}}{Cd^2}$. Here A is the area of the suspended graphene region and d is the separation between the graphene membrane and its cavity counter electrode. In order to optimize the coupling g_0, it is crucial to minimize both C and d. To this end, we utilize a narrow cavity conductor structured in a meander to increase L, while minimizing the capacitance to the ground for a given $\omega_{\rm c}$. In order to be able to tune d with $V_{\rm g}^{\rm DC}$, we use a cavity that is shorted to ground on one side, allowing for a well defined electrical DC potential. The fundamental mode of the cavity is a quarter wavelength standing wave, with a voltage node at the shorted end and the largest voltage oscillation amplitudes at

the open end. The graphene membrane is coupled close to the open end of the cavity to harness the largest cavity fields (see Fig. 1b,c) [23, 28, 29]. Using this geometry, we achive a cavity capacitance of $C \approx 90$ fF. This compares favorably with $C = 18$ fF-1 pF in previous studies [12, 23–27]. Note that the lowest values for C have been achieved in closed-loop cavities, where the mechanical capacitance is incorporated between the two ends of a half-wavelength cavity [12, 26]. In this geometry the two electrodes of the mechanical capacitance are shorted over the cavity, so that no static DC potential can be applied. Compared to the capacitance of a gated half-wavelength cavities [30–32], the capacitance of a quarter wavelength cavity is lowered by a factor of two.

We use a graphene resonator with a circular shape. This geometry improves the attachment of the graphene sheet to its support when compared to the doubly-clamped resonator geometry. As further discussed below, a strong attachment of the graphene to its support is crucial to be able to lower d. Another advantage of circular graphene resonators over doubly-clamped resonators is that the quality factor tends to be larger [33]. In addition, the mechanical eigenmodes of circular resonators are well defined [33, 34]. In particular, it avoids the formation of modes localized at the edges, which were observed in doubly-clamped resonators [35].

To fabricate the devices, we start by carving out the superconducting cavity structure from a 200 nm thick sputtered Niobium (Nb) film by ion milling and reactive ion etching (see SI). We employ a PMMA supported transfer technique pioneered at Columbia [36] to position graphene flakes on the superconducting cavity structure. For this, we exfoliate graphene sheets from large graphite crystals onto a silicon (Si) chip covered by a polymer film consisting of 100 nm polyvinyl alcohol (PVA) and 200 nm PMMA 495K. The thickness of the PVA/PMMA film is optimized to give the largest optical contrast of graphene flakes in an optical microscope. In particular, it allows to calibrate the number of layers of the graphene flake [37, 38]. The solvability of PVA in water is used to separate the Si chip from the PMMA with the graphene. Using a brass slide with a volcano-shaped hole, the membrane is fished from the water and dryed on a hotplate. When drying, the PMMA membrane gets uniformely stretched across the volcano hole. By mounting the slide upside down into a micromanipulator, the graphene sheet can be aligned and transferred onto the pre-patterned superconducting cavity structure, as illustrated in Fig. 2a. To improve the attachment of the graphene flake to its support, it was shown that it is important to clamp

the graphene membrane on the two sides of its surface [39]. For this, we crosslink part of the transferred PMMA with a 10′000 μC/cm^2 electron beam dose (Fig. 2b). The unexposed PMMA is removed in 80°C hot N-Methyl-2-pyrrolidone (NMP), followed by critical point drying of the device. As a result, the graphene is firmly sandwiched between the support electrode and the crosslinked PMMA (Fig. 2c,d). Using this technique the graphene sheet is less likely to collapse against its counter electrode. This allows to increase the success yield of the device fabrication. We have succesfully lowered the separation to $d = 85$ nm for a 3.5 μm diameter graphene resonator, which is equal to the best diameter-separation ratio of $2R/d = 40$ reported so far for graphene resonators [40]. In addition, the strong attachment between the graphene and its support allows us to electrostatically tune the equilibrium position by a large amount (see below).

In this letter we present results measured at 30 mK for two different graphene devices, hereafter called devices A and B. Device A is a three layer graphene resonator with radius $R = 1.75$ μm and with $d = 95$ nm. The number of layers is determined from optical contrast measurements. The radius of the counter electrode is $R_{\rm g} = 1.1$ μm (see Fig. 2d). Device B is a four layer graphene resonator with the same membrane radius, $d = 135$ nm and $R_{\rm g} = 1.25$ μm.

In order to detect the vibrations of the graphene resonator, we couple the open-end of the superconducting cavity to a microwave transmission line through the capacitance $C_{\rm ext}$. The transmission line is used to pump the superconducting cavity at frequency $\omega_{\rm p}/2\pi$ with input power $P_{\rm p,in}$. The transmission line is also employed to measure the output power $P_{\rm out}$ of the cavity at the frequency $\omega_{\rm c}/2\pi$. $P_{\rm out}$ is amplified by a high-electron-mobility transistor (HEMT) at 4 K and measured in a spectrum analyzer (see schematic in Fig. 1d). The principle of the vibration readout is analogous to Stokes and anti-Stokes Raman scattering. By pumping the cavity at $\omega_{\rm p}$, sidebands in energy are created at $\omega_{\rm p} \pm \omega_{\rm m}$ due to the coupling of the photons with the mechanical motion. If the pump is detuned such that the upper sideband frequency is matched with the cavity resonance frequency $\omega_{\rm c} = \omega_{\rm p} + \omega_{\rm m}$ (see Fig. 1e), the anti-Stokes scattering is resonantly enhanced. If $\omega_{\rm m}$ is significantly larger than the linewidth κ of the cavity, the rate of the anti-Stokes scattering per phonon is given by $\Gamma_+ \approx 4n_{\rm p}g_0^2/\kappa$, with $n_{\rm p} \propto P_{\rm p,in}(\omega_{\rm p})$ the number of photons in the cavity. We drive the graphene resonator by applying a constant voltage $V_{\rm g}^{\rm DC}$ and an oscillating voltage with amplitude $V_{\rm g}^{\rm AC}$ at a frequency $\omega_{\rm d}/2\pi$ close to $\omega_{\rm m}/2\pi$ so that $\omega_{\rm d} = \omega_{\rm c} - \omega_{\rm p}$. As a result, the

graphene resonator vibrates at $z(t) = \hat{z}\cos(\omega_{\rm d}t + \phi)$ with ϕ the phase difference between the displacement and the driving force. The output power at $\omega_{\rm c}$ is

$$P_{\rm out} = P_{\rm p,in}\frac{\kappa_{ext}^2}{\kappa^2 + 4(\omega_{\rm c} - \omega_{\rm p})^2}4\frac{g_0^2}{\kappa^2}\frac{\langle z(t)^2\rangle}{2z_{\rm zp}^2}. \quad (1)$$

From a transmission measurement of the feedline we readily get the resonance frequency of the cavity $\omega_{\rm c}/2\pi = 6.728$ GHz and the total linewidth $\kappa/2\pi = \kappa_{\rm ext}/2\pi + \kappa_{\rm int}/2\pi = 15$ MHz with $\kappa_{\rm ext}/2\pi = 2$ MHz the coupling rate of the superconducting cavity to the feedline and $\kappa_{\rm int}/2\pi = 13$ MHz the internal loss rate of the cavity. For device B we have $\omega_{\rm c}/2\pi = 6.69$ GHz, $\kappa/2\pi = 17$ MHz, $\kappa_{\rm int}/2\pi = 15$ MHz, $\kappa_{\rm ext}/2\pi = 2$ MHz.

Fig. 3a,b show the resonance of the driven vibrations for the fundamental modes of device A and B; modes at higher frequencies are observed as well, but they are hardly detectable. For device A we extract the mechanical quality factor $Q_{\rm m} = \omega_{\rm m}/\gamma_{\rm m} \approx 100'000$ from the linewidth of the resonance $\gamma_{\rm m}/2\pi = 575$ Hz, which is measured with $n_{\rm p} = 8000$ photons. This $Q_{\rm m}$ is comparable to the largest values reported thus far for graphene resonators [41], showing that our fabrication process does provide us with mechanical resonators of excellent quality. In device B we measure a quality factor of $Q_{\rm m} = 17'700$. We attribute this lower $Q_{\rm m}$ to the fact that the device was imaged in a scanning electron microscope (SEM) before the measurements, where the graphene surface got contaminated by amorphous carbon.

The resonance frequency decreases upon increasing $|V_{\rm g}^{\rm DC}|$ (see Fig. 3c,d). This reduction of the resonance frequency has been observed previously in graphene resonators under tension [41–43]. This softening of the resonator is attributed to the change of the restoring potential of the resonator by the capacitive energy [41–44]. We model the mechanical resonator with a circular membrane under tension [45] to quantify the observed dependence. When neglecting static deflection, the frequency dependence is given by

$$\omega_{\rm m}(V_{\rm g}^{\rm DC}) = \sqrt{\frac{4.92Eh\epsilon}{m_{\rm eff}} - \frac{0.271}{m_{\rm eff}}\frac{\epsilon_0\pi R_{\rm g}^2}{d^3}(V_{\rm g}^{\rm DC})^2}, \quad (2)$$

with ϵ the strain in the graphene sheet, $E \approx 1$ TPa the Youngs modulus of graphite, $h = n_{\rm g}\times 0.34$ nm the graphene thickness, $n_{\rm g}$ the number of graphene layers [3, 42] and $m_{\rm eff} = 0.27\pi R^2\rho_{\rm 2D}$ the effective mass of the fundamental mode (see SI). The two dimensional mass density $\rho_{\rm 2D} = \eta n_{\rm g}\rho_{\rm graphene}$ includes the graphene mass density $\rho_{\rm graphene} = 7.6\times 10^{-19}$ kg/μm^2 and a correction factor $\eta \geq 1$ to account for contamination on the graphene surface. From a fit of Eq. (2) to the measurements around $V_{\rm g}^{\rm DC} = 0$ (in Fig. 3c,d), we extract $m_{\rm eff} =$

$13 \cdot 10^{-18}$ kg and $\epsilon = 0.036\%$ for device A, and $m_{\rm eff} = 36 \cdot 10^{-18}$ kg and $\epsilon = 0.024\%$ for device B. The obtained mass is $\eta = 2.2$ times larger than the total graphene mass for device A and $\eta = 4.5$ times larger for device B. The larger η for device B might be attributed to the amorphous carbon deposited during SEM inspection. The tension is intermediate compared to previous measurements, where ϵ ranges from 0.002% to 1% [3, 33, 41, 46].

In order to account for the variation of $\omega_{\rm m}$ for large $V_{\rm g}^{\rm DC}$ in Fig. 3c,d, the static deflection of the graphene sheet towards the cavity counter electrode has to be considered. The static displacement of the center of the membrane $z_{\rm s}$ is given by

$$z_{\rm s} = \frac{\epsilon_0 R_{\rm g}^2}{8Eh\epsilon d^2}(V_{\rm g}^{\rm DC})^2 = c_{\rm s}(V_{\rm g}^{\rm DC})^2 \tag{3}$$

for small displacement compared to d. Although the renormalization of the mechanical frequency due to static displacement cannot be solved exactly, as an approximation we can include $z_{\rm s}$ in Eq. (2) using $d = d_0 - z_{\rm s}$, with d_0 the separation for $V_{\rm g}^{\rm DC} = 0$. We get a good agreement for $\omega_{\rm m}(V_{\rm g}^{\rm DC})$ between the measurements and theory without any fitting parameter over the $V_{\rm g}^{\rm DC}$ range shown in Fig. 3c,d. The effect of $z_{\rm s}$ on the shift in $\omega_{\rm m}$ is 42% at $V_{\rm g}^{\rm DC} = -6$ V for device A and 10% at $V_{\rm g}^{\rm DC} = 4$ V for device B. The expected variation of $z_{\rm s}$ is plotted in Fig. 4a.

The softening of the graphene resonator becomes enormous upon further increasing $V_{\rm g}^{\rm DC}$, with a reduction of $\omega_{\rm m}$ by a factor of three down to ≈ 10 MHz as shown in Fig. 4b for device B. This reduction of $\omega_{\rm m}$ is large compared to that measured in previous works [42–44]. Even though further work is needed to understand this dependence, it reveals that the graphene resonators we fabricate can bend by a large amount without being riped apart due to the large induced strain and without sliding with respect to the anchor electrodes.

Our device layout allows us to get large couplings g_0 between the mechanical resonator and the superconducting cavity (Fig. 3e,f). We extract g_0 from the measurements of the response of driven vibrations at $\omega_{\rm d} = \omega_{\rm m}$ using Eq. (1) where $\langle z(t)^2 \rangle = [\partial_{\rm z} C_{\rm m} \cdot V_{\rm g}^{\rm DC} V_{\rm g}^{\rm AC} Q_{\rm m}/(m_{\rm eff}\omega_{\rm m}^2)]^2$. Remarkably, g_0 gets larger upon increasing $|V_{\rm g}^{\rm DC}|$ for device A. This tunability of g_0 is attributed to the static deflection of the graphene sheet. When incorporating the effect of the static displacement into $C_{\rm m}$, we get a good agreement between the expected $g_0 = \omega_{\rm c}/(2C) \cdot \partial_{\rm z} C_{\rm m}$ and the measurements, using $C = 75$ fF and 100 fF for devices A and B, respectively (red lines in Fig. 3e,f). These values of C agree well with $C = 90$ fF estimated from simulations. The obtained coupling rates g_0 compare favourably with previous experiments

carried out with mechanical resonators made from other materials. Indeed, the coupling was $g_0/2\pi \sim 1$ Hz in works with cavity geometries similar to ours [25, 27, 47]. Larger values were achieved with closed-loop cavities ($g_0/2\pi = 40$ and 210 Hz) but this geometry does not allow to apply $V_{\rm g}^{\rm DC}$ between the mechanical resonator and a counter electrode as discussed above [12, 26].

Now, we investigate how the strong tunability of the graphene equilibrium position affects the nonlinear response of the mechanical resonator. For this, we measure the displacement as a function of $\omega_{\rm d}$ for large driving forces at different $V_{\rm g}^{\rm DC}$. Interestingly, we are able to tune the sign of the Duffing nonlinearity from a hardening behavior at low $V_{\rm g}^{\rm DC}$ (Fig. 5a) to a softening behavior at high $V_{\rm g}^{\rm DC}$ (Fig. 5c). At an intermediate $V_{\rm g}^{\rm DC}$ of about 3.4 V, we are able to cancel the Duffing nonlinearity, that is, the resonant frequency remains roughly constant upon varying the driving force (Fig. 5b). We quantify the Duffing nonlinearity from the critical displacement amplitude $\hat{z}_{\rm crit}$ above which the response gets bistable. For a Duffing resonator with linear damping, the effective Duffing constant $\alpha_{\rm eff}$ is related to $\hat{z}_{\rm crit}$ by $\alpha_{\rm eff} = \frac{8}{3\sqrt{3}} m_{\rm eff}\omega_{\rm m}^2/(Q_{\rm m}\hat{z}_{\rm crit})$ [48]. Figure 5d shows that $\alpha_{\rm eff}$ is positive at low $V_{\rm g}^{\rm DC}$ and becomes negative at large $V_{\rm g}^{\rm DC}$. This dependence can be attributed to the symmetry breaking of the mechanical motion induced by static deflection [49], which reads

$$\alpha_{\rm eff} \approx \alpha_0 - \frac{10}{m_{\rm eff}\omega_{\rm m}^2}\alpha_0^2 z_{\rm s}^2 \tag{4}$$

where α_0 is the Duffing constant when $V_{\rm g}^{\rm DC} = 0$; α_0 could have a geometrical origin [48]. The fit of Eq. (4) to the measurement yields $c_{\rm s} = 0.65$ nm/V^2 and $\alpha_0 = 1.9 \cdot 10^{15}$ kgm^{-2}s^{-2} (red line in Fig. 5d). This value of $c_{\rm s}$ is consistent with that expected from Eq. (3). The sign change of the Duffing nonlinearity due to static deformation is a unique property of graphene and nanotube resonators [50].

The prospects to reach the quantum regime with graphene resonators are promising. For this, it is illustrative to compare the figures of merit achieved here to those reported by Teufel *et al.* [12], which allowed to demonstrate ground-state cooling with a superconducting cavity. In the device A of our work, we measure $g_0/2\pi \approx 15$ Hz, $n_{\rm p} = 8000$, $Q_{\rm m} = 100'000$ and $\kappa_{\rm int}/2\pi = 13$ MHz, while the parameters of Teufel *et al.* are $g_0/2\pi \approx 200$ Hz, $n_{\rm p} = 4000$, $Q_{\rm m} = 350'000$ and $\kappa_{\rm int}/2\pi = 40$ kHz. The high $\kappa_{\rm int}$ in our device might be attributed to losses due to either contamination during the transfer step or the electrical connections used to apply $V_{\rm g}^{\rm DC}$ and $V_{\rm g}^{\rm AC}$ on the graphene electrodes. Indeed, we measure much smaller

losses in a cavity where no transfer is performed and the graphene electrodes are grounded ($\kappa_{\rm int}/2\pi \approx 200$ kHz). Here, more work is needed to improve $\kappa_{\rm int}$. In order to increase g_0, we will reduce d further by fabrication and graphene pulling. We should reach $g_0/2\pi \approx 250$ Hz with $d = 30$ nm. An alternative route to increase g_0 is to enhance the coupling using a cooper-pair box [51, 52].

In conclusion, we have reported devices where a graphene resonator is coupled to a superconducting cavity. The tunability of these devices, in combination with the large graphene-cavity coupling, constitutes a promising approach to study quantum motion. The large reduction of the resonance frequency of the graphene resonator observed here is interesting to enhance the zero-point motion and to increase the effect of mechanical nonlinearities [53–55]. The tunability of the resonance frequency with $V_{\rm g}^{\rm DC}$ is suitable for parametric amplification and quantum squeezing of mechanical states [56]. In these graphene-cavity devices, the opto-mechanical coupling can be varied not only with the number of photons but also with $V_{\rm g}^{\rm DC}$. Because the mass of graphene is ultra-low, its motion is extremely sensitive to changes in the environment. It will be interesting to couple the quantum vibrations of motion to other degrees of freedom, such as electrons and spins.

Acknoledgements

We would like to thank Joel Moser, Gabriel Puebla, Christopher Eichler, Andreas Isacsson, Martin Eriksson, Sara Hellmüller and Andreas Wallraff for helpfull discussions. We gratefully acknowledge Gustavo Ceballos and the ICFO mechanical and electronic workshop for support. We acknowledge support from the European Union through the RODIN-FP7 project, the ERC-carbonNEMS project, and the Graphene Flagship (grant agreement 604391), the Spanish state (MAT2012-31338), the Catalan government (AGAUR, SGR).

Author contributions

P.W, J.G. and I.T. developed the fabrication process. P.W. fabricated the devices with support from J.G. The experimental setup was built up by J.G. with support from P.W. P.W and J.G. carried out the measurements. J.G. and P.W analyzed the data with support from A.B. and D.E.C. J.G and A.B. wrote the manuscript with critical comments from all authors. A.B and J.G conceived the experiment and supervised the work.

References

[1] H.-Y. Chiu, P. Hung, H. W. C. Postma, and M. Bockrath, Nano Letters **8**, 4342 (2008), http://pubs.acs.org/doi/pdf/10.1021/nl802181c, URL http://pubs.acs.org/doi/abs/10.1021/nl802181c.

[2] J. Chaste, A. Eichler, J. Moser, G. Ceballos, R. Rurali, and A. Bachtold, Nature nanotechnology **7**, 301 (2012).

[3] J. S. Bunch, A. M. Van Der Zande, S. S. Verbridge, I. W. Frank, D. M. Tanenbaum, J. M. Parpia, H. G. Craighead, and P. L. McEuen, Science **315**, 490 (2007), URL http://www.sciencemag.org/content/315/5811/490.

[4] J. Moser, J. Güttinger, A. Eichler, M. Esplandiu, D. Liu, M. Dykman, and A. Bachtold, Nature Nanotechnology **8**, 493496 (2013).

[5] S. Stapfner, L. Ost, D. Hunger, J. Reichel, I. Favero, and E. M. Weig, Applied Physics Letters **102**, 151910 (2013), URL http://scitation.aip.org/content/aip/journal/apl/102/15/10.1063/1.4802746.

[6] A. Eichler, J. Chaste, J. Moser, and A. Bachtold, Nano letters **11**, 2699 (2011).

[7] A. Ayari, P. Vincent, S. Perisanu, M. Choueib, V. Gouttenoire, M. Bechelany, D. Cornu, and S. T. Purcell, Nano Letters **7**, 2252 (2007), pMID: 17608540, http://pubs.acs.org/doi/pdf/10.1021/nl070742r, URL http://pubs.acs.org/doi/abs/10.1021/nl070742r.

[8] C. Chen, S. Lee, V. V. Deshpande, G.-H. Lee, M. Lekas, K. Shepard, and J. Hone, Nature nanotechnology **8**, 923 (2013), URL http://www.nature.com/nnano/journal/v8/n12/abs/nnano.2013.232.html.

[9] M. Poot and H. S. van der Zant, Physics Reports **511**, 273 (2012), URL http://www.sciencedirect.com/science/article/pii/S0370157311003644.

[10] M. Aspelmeyer, T. J. Kippenberg, and F. Marquardt, arXiv preprint arXiv:1303.0733 (2013), URL http://arxiv.org/abs/1303.0733.

[11] A. D. OConnell, M. Hofheinz, M. Ansmann, R. C. Bialczak, M. Lenander, E. Lucero, M. Neeley, D. Sank, H. Wang, M. Weides, et al., Nature **464**, 697 (2010).

[12] J. Teufel, T. Donner, D. Li, J. Harlow, M. Allman, K. Cicak, A. Sirois, J. Whittaker, K. Lehnert, and R. Simmonds, Nature **475**, 359363 (2011).

[13] J. Chan, T. M. Alegre, A. H. Safavi-Naeini, J. T. Hill, A. Krause, S. Gröblacher, M. Aspelmeyer, and O. Painter, Nature **478**, 89 (2011).

[14] N. Kiesel, F. Blaser, U. Delić, D. Grass, R. Kaltenbaek, and M. Aspelmeyer, Proceedings of the National Academy of Sciences **110**, 14180 (2013), URL http://www.pnas.org/content/110/35/14180.short.

[15] J. Gieseler, L. Novotny, and R. Quidant, Nature Physics **9**, 806 (2013).

[16] K.-K. Ni, R. Norte, D. J. Wilson, J. D. Hood, D. E. Chang, O. Painter, and H. J. Kimble, Phys. Rev. Lett. **108**, 214302 (2012), URL http://link.aps.org/doi/10.1103/PhysRevLett.108.214302.

[17] A. G. Kuhn, M. Bahriz, O. Ducloux, C. Chartier, O. Le Traon, T. Briant, P.-F. Cohadon, A. Heidmann, C. Michel, L. Pinard, et al., Applied Physics Letters **99**, 121103 (2011), URL http://scitation.aip.org/content/aip/journal/apl/99/12/10.1063/1.3641871.

[18] T. Bagci, A. Simonsen, S. Schmid, L. Villanueva, E. Zeuthen, J. Appel, J. Taylor, A. Sørensen, K. Usami, A. Schliesser, et al., Nature **507**, 81 (2013), URL http://www.nature.com/nature/journal/v507/n7490/full/nature13029.html.

[19] R. Andrews, R. Peterson, T. Purdy, K. Cicak, R. Simmonds, C. Regal, and K. Lehnert, arXiv preprint arXiv:1310.5276 (2013), URL http://arxiv.org/abs/1310.5276.

[20] L. Ding, C. Baker, P. Senellart, A. Lemaitre, S. Ducci, G. Leo, and I. Favero, Phys. Rev. Lett. **105**, 263903 (2010), URL http://link.aps.org/doi/10.1103/PhysRevLett.105.263903.

[21] I. Yeo, P.-L. de Assis, A. Gloppe, E. Dupont-Ferrier, P. Verlot, N. S. Malik, E. Dupuy, J. Claudon, J.-M. Gérard, A. Auffèves, et al., Nature nanotechnology **9**, 106 (2013), URL http://www.nature.com/nnano/journal/v9/n2/full/nnano.2013.274.html.

[22] R. A. Barton, I. R. Storch, V. P. Adiga, R. Sakakibara, B. R. Cipriany, B. Ilic, S. P. Wang, P. Ong, P. L. McEuen, J. M. Parpia, et al., Nano Letters **12**, 4681 (2012), http://pubs.acs.org/doi/pdf/10.1021/nl302036x, URL http://pubs.acs.org/doi/abs/10.1021/nl302036x.

[23] C. Regal, J. Teufel, and K. Lehnert, Nature Physics **4**, 555 (2008).

[24] J. Hertzberg, T. Rocheleau, T. Ndukum, M. Savva, A. Clerk, and K. Schwab, Nature Physics **6**, 213 (2009).

[25] T. Rocheleau, T. Ndukum, C. Macklin, J. Hertzberg, A. Clerk, and K. Schwab, Nature **463**, 72 (2010).

[26] F. Massel, T. Heikkilä, J.-M. Pirkkalainen, S. Cho, H. Saloniemi, P. Hakonen, and M. Sillanpää, Nature **480**, 351 (2011).

[27] X. Zhou, F. Hocke, A. Schliesser, A. Marx, H. Huebl, R. Gross, and T. Kippenberg, Nature Physics **9**, 179 (2013), URL `http://www.nature.com/nphys/journal/v9/n3/full/nphys2527.html`.

[28] P. K. Day, H. G. LeDuc, B. A. Mazin, A. Vayonakis, and J. Zmuidzinas, Nature **425**, 817 (2003).

[29] J. Teufel, T. Donner, M. Castellanos-Beltran, J. Harlow, and K. Lehnert, Nature nanotechnology **4**, 820 (2009).

[30] M. R. Delbecq, V. Schmitt, F. D. Parmentier, N. Roch, J. J. Viennot, G. Fève, B. Huard, C. Mora, A. Cottet, and T. Kontos, Phys. Rev. Lett. **107**, 256804 (2011), URL `http://link.aps.org/doi/10.1103/PhysRevLett.107.256804`.

[31] T. Frey, P. J. Leek, M. Beck, A. Blais, T. Ihn, K. Ensslin, and A. Wallraff, Phys. Rev. Lett. **108**, 046807 (2012), URL `http://link.aps.org/doi/10.1103/PhysRevLett.108.046807`.

[32] K. Petersson, L. McFaul, M. Schroer, M. Jung, J. Taylor, A. Houck, and J. Petta, Nature **490**, 380 (2012), URL `http://www.nature.com/nature/journal/v490/n7420/full/nature11559.html`.

[33] R. A. Barton, B. Ilic, A. M. van der Zande, W. S. Whitney, P. L. McEuen, J. M. Parpia, and H. G. Craighead, Nano Letters **11**, 1232 (2011), http://pubs.acs.org/doi/pdf/10.1021/nl1042227, URL `http://pubs.acs.org/doi/abs/10.1021/nl1042227`.

[34] A. Eriksson, D. Midtvedt, A. Croy, and A. Isacsson, Nanotechnology **24**, 395702 (2013), URL `http://iopscience.iop.org/0957-4484/24/39/395702`.

[35] D. Garcia-Sanchez, A. M. van der Zande, A. S. Paulo, B. Lassagne, P. L. McEuen, and A. Bachtold, Nano Letters **8**, 1399 (2008), pMID: 18402478, http://pubs.acs.org/doi/pdf/10.1021/nl080201h, URL `http://pubs.acs.org/doi/abs/10.1021/nl080201h`.

[36] C. Dean, A. Young, I. Meric, C. Lee, L. Wang, S. Sorgenfrei, K. Watanabe, T. Taniguchi, P. Kim, K. Shepard, et al., Nature nanotechnology **5**, 722 (2010).

[37] P. Blake, E. W. Hill, A. H. Castro Neto, K. S. Novoselov, D. Jiang, R. Yang, T. J. Booth, and A. K. Geim, Applied Physics Letters **91**, 063124 (2007), URL http://scitation.aip.org/content/aip/journal/apl/91/6/10.1063/1.2768624.

[38] Z. H. Ni, H. M. Wang, J. Kasim, H. M. Fan, T. Yu, Y. H. Wu, Y. P. Feng, and Z. X. Shen, Nano Letters **7**, 2758 (2007), http://pubs.acs.org/doi/pdf/10.1021/nl071254m, URL http://pubs.acs.org/doi/abs/10.1021/nl071254m.

[39] W. Bao, K. Myhro, Z. Zhao, Z. Chen, W. Jang, L. Jing, F. Miao, H. Zhang, C. Dames, and C. N. Lau, Nano letters **12**, 5470 (2012), URL http://pubs.acs.org/doi/abs/10.1021/nl301836q.

[40] S. Lee, C. Chen, V. V. Deshpande, G.-H. Lee, I. Lee, M. Lekas, A. Gondarenko, Y.-J. Yu, K. Shepard, P. Kim, et al., Applied Physics Letters **102**, 153101 (2013), URL http://scitation.aip.org/content/aip/journal/apl/102/15/10.1063/1.4793302.

[41] A. Eichler, J. Moser, J. Chaste, M. Zdrojek, I. Wilson-Rae, and A. Bachtold, Nature Nanotechnology **6**, 339 (2011).

[42] C. Chen, S. Rosenblatt, K. Bolotin, W. Kalb, P. Kim, I. Kymissis, H. Stormer, T. Heinz, and J. Hone, Nature nanotechnology **4**, 861 (2009).

[43] X. Song, M. Oksanen, M. A. Sillanpää, H. Craighead, J. Parpia, and P. J. Hakonen, Nano Letters **12**, 198 (2011).

[44] I. Kozinsky, H. W. C. Postma, I. Bargatin, and M. L. Roukes, Applied Physics Letters **88**, 253101 (2006), URL http://scitation.aip.org/content/aip/journal/apl/88/25/10.1063/1.2209211.

[45] L. D. Landau, E. Lifshitz, J. Sykes, W. Reid, and E. H. Dill, *Theory of elasticity: Vol. 7 of course of theoretical physics* (Pergamon Press, 1970), 2nd ed.

[46] C. Chen and J. Hone, Proceedings of the IEEE **101**, 1766 (2013), ISSN 0018-9219.

[47] J. D. Teufel, J. W. Harlow, C. A. Regal, and K. W. Lehnert, Phys. Rev. Lett. **101**, 197203 (2008).

[48] R. Lifshitz and M. Cross, Reviews of nonlinear dynamics and complexity **1**, 1 (2008).

[49] M. Younis and A. Nayfeh, Nonlinear Dynamics **31**, 91 (2003), ISSN 0924-090X, URL http://dx.doi.org/10.1023/A%3A1022103118330.

[50] A. Eichler, M. del Álamo Ruiz, J. A. Plaza, and A. Bachtold, Phys. Rev. Lett. **109**, 025503 (2012), URL http://link.aps.org/doi/10.1103/PhysRevLett.109.025503.

[51] T. T. Heikkilä, F. Massel, J. Tuorila, R. Khan, and M. A. Sillanpää, arXiv preprint arXiv:1311.3802 (2013), URL http://arxiv.org/abs/1311.3802.

[52] A. Rimberg, M. Blencowe, A. Armour, and P. Nation, arXiv preprint arXiv:1312.7521 (2013), URL http://arxiv.org/abs/1312.7521.

[53] A. Voje, J. M. Kinaret, and A. Isacsson, Phys. Rev. B **85**, 205415 (2012), URL http://link.aps.org/doi/10.1103/PhysRevB.85.205415.

[54] S. Rips and M. J. Hartmann, Phys. Rev. Lett. **110**, 120503 (2013), URL http://link.aps.org/doi/10.1103/PhysRevLett.110.120503.

[55] S. Rips, I. Wilson-Rae, and M. J. Hartmann, Phys. Rev. A **89**, 013854 (2014), URL http://link.aps.org/doi/10.1103/PhysRevA.89.013854.

[56] X.-Y. Lü, J.-Q. Liao, L. Tian, and F. Nori, arXiv preprint arXiv:1403.0049 (2014), URL http://arxiv-web3.library.cornell.edu/abs/1403.0049.

Figures

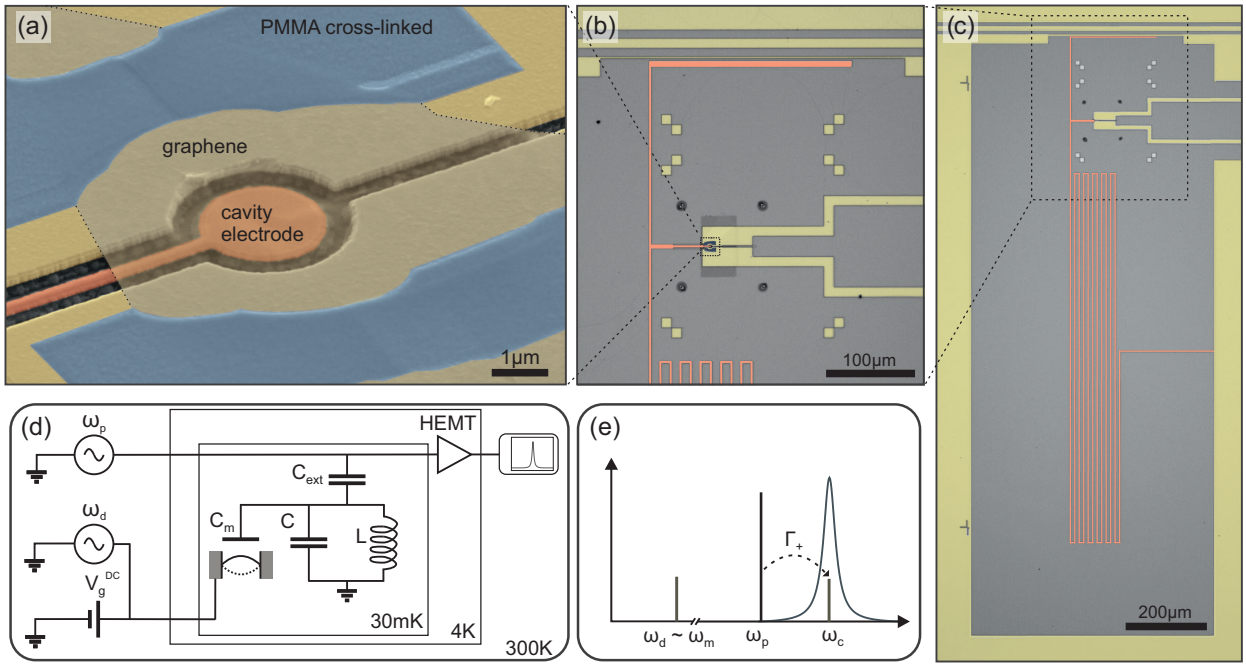

FIG. 1: (a) False color SEM image of a circular graphene resonator capacitively coupled to a cavity electrode (red). The graphene sheet is clamped inbetween cross-linked PMMA (blue) and graphene support electrodes (yellow). (b,c) Optical microscope images of the superconducting cavity (red), two electrodes contacting the graphene flake (yellow, situated on the right-side of b and c), and a capacitively coupled transmission line (yellow, situated at the top in b and c). (d) Measurement schematic for the detection of the mechanical motion. Coherent pump $\omega_{\rm p}$ and drive $\omega_{\rm d}$ fields are applied to the transmission line and the graphene mechanical resonator, respectively. A constant voltage $V_{\rm g}^{\rm DC}$ is applied to the graphene. The microwave signal from the cavity is amplified at 4 K with a HEMT amplifier and recorded at room temperature with a spectrum analyzer. (e) If the pump frequency is detuned such that $\omega_{\rm p} = \omega_{\rm c} - \omega_{\rm d}$, anti-Stokes scattering with phonons at rate Γ_+ leads to a detectable photon population at $\omega_{\rm c}$.

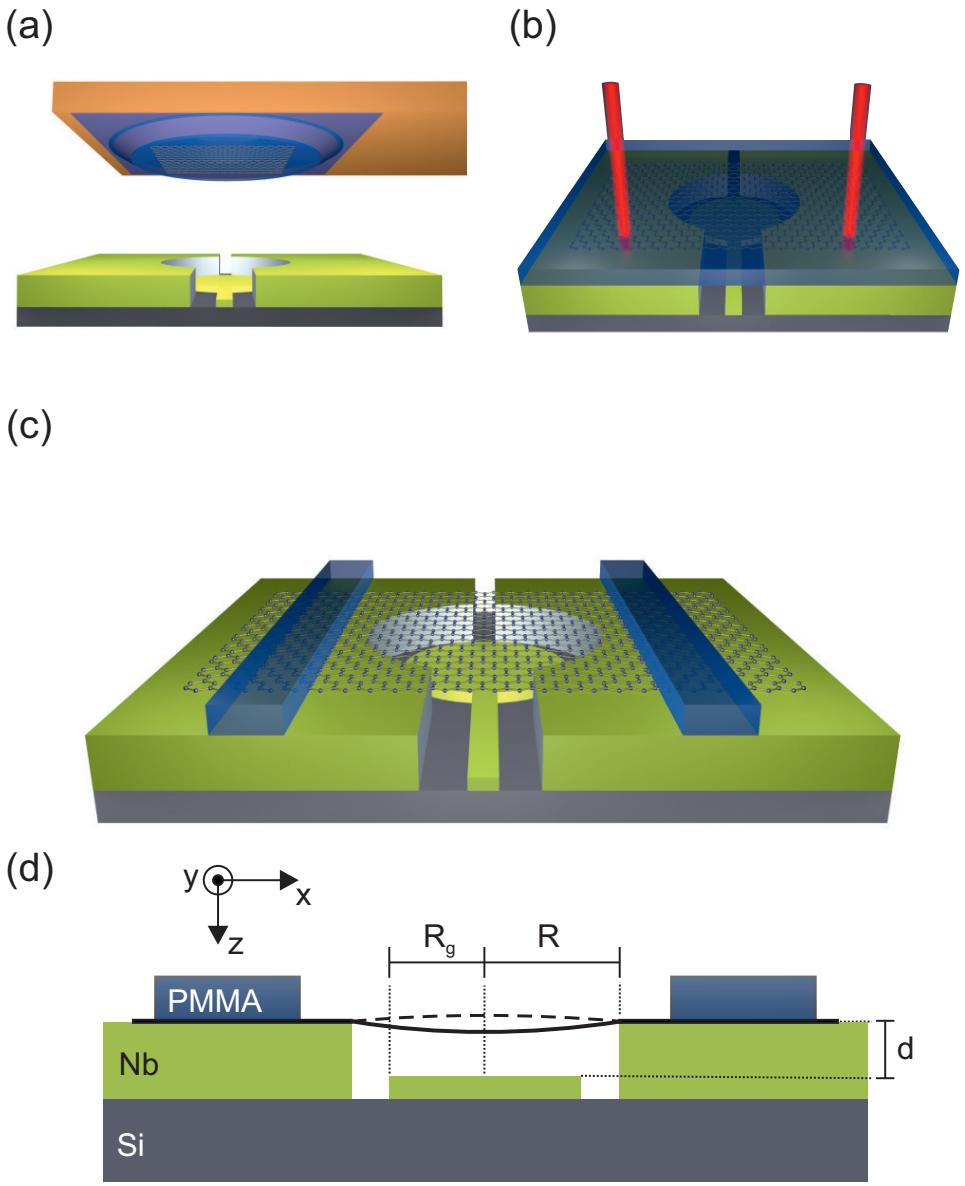

FIG. 2: Fabrication process for PMMA-clamped graphene mechanical resonator. (a) Transfer of graphene with PMMA (blue) onto predefined structure (yellow, gray). (b) Cross-linking part of the transferred PMMA by electron-beam overexposure (red). (c) Schematic of the final device. (d) Cross-section of the device.

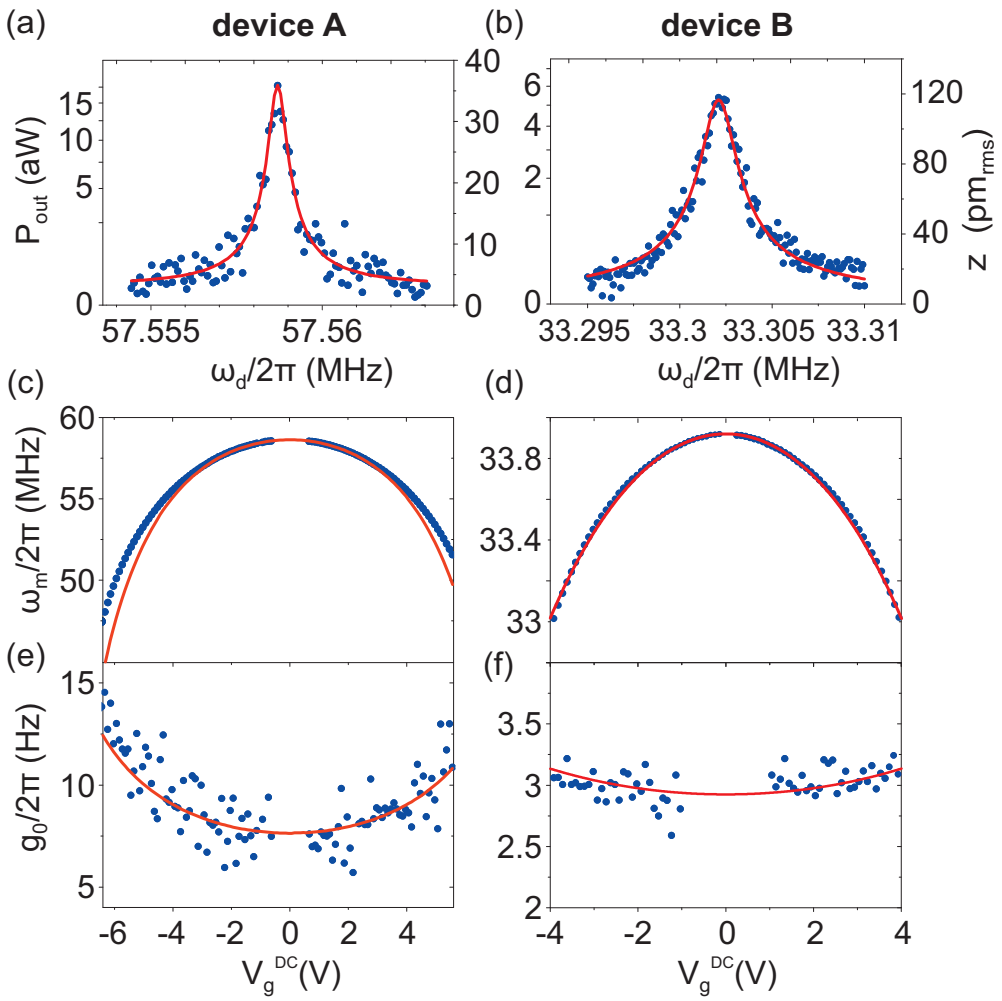

FIG. 3: (a),(b) Sideband measurement of the mechanical motion for device A with $V_{\mathrm{g}}^{\mathrm{DC}} = -2.894$ V and $V_{\mathrm{g}}^{\mathrm{AC}} = 190$ nV, and for device B with $V_{\mathrm{g}}^{\mathrm{DC}} = 3.405$ V and $V_{\mathrm{g}}^{\mathrm{AC}} = 4.3$ μV. Red lines are lorentzian fits to the data which yield a mechanical quality factor of $Q_{\mathrm{m}} = 100'000$ in device A and $Q_{\mathrm{m}} = 17'700$ in device B. The calculated motional rms amplitude z is plotted on the right scale. (c),(d) Mechanical resonance frequency as a function of $V_{\mathrm{g}}^{\mathrm{DC}}$. We have compensated $V_{\mathrm{g}}^{\mathrm{DC}}$ by an offset of 0.434 V for device A and 0.395 V for device B. In addition to capacitive softening, the static deflection z_{s} of the resonator towards the cavity counter electrode is considered in order to account for the measurement (red line). (e),(f) Single-photon coupling rate $g_0 = G_0 z_{\mathrm{zp}}$. By including the static displacement z_{s} we are able to model the single-photon coupling as a function of $V_{\mathrm{g}}^{\mathrm{DC}}$ (red line).

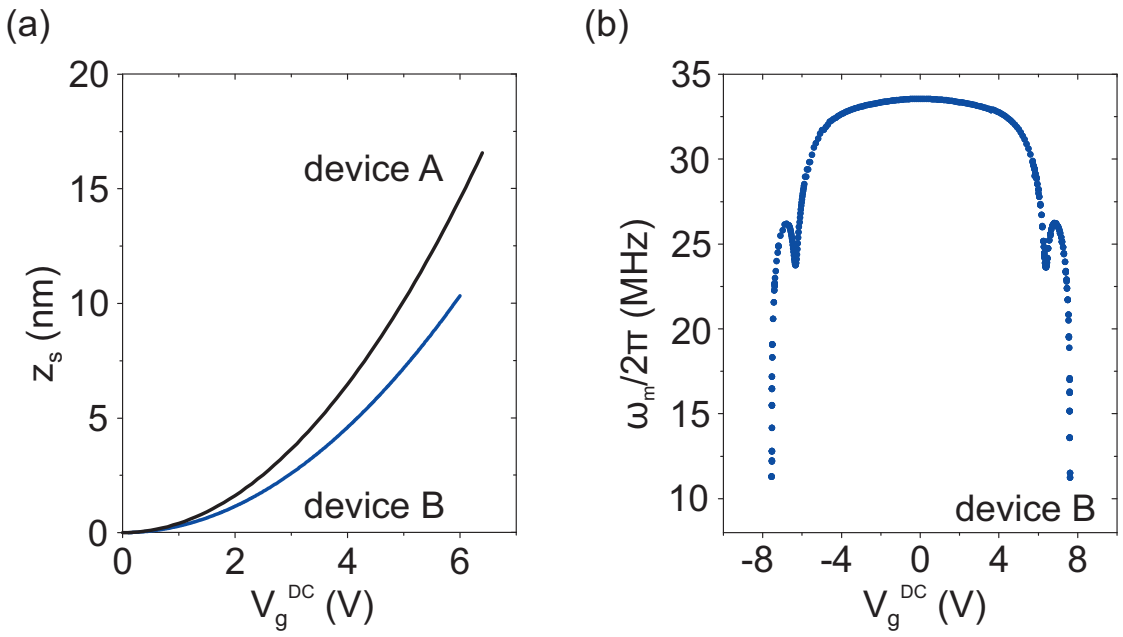

FIG. 4: (a) Static displacement of the center of the membrane calculated from Eq. (3) with constants $c_s = 0.405$ nm/V^2 for device A and $c_s = 0.287$ nm/V^2 for device B. (b) Mechanical resonance frequency as a function of V_g^{DC} for device B.

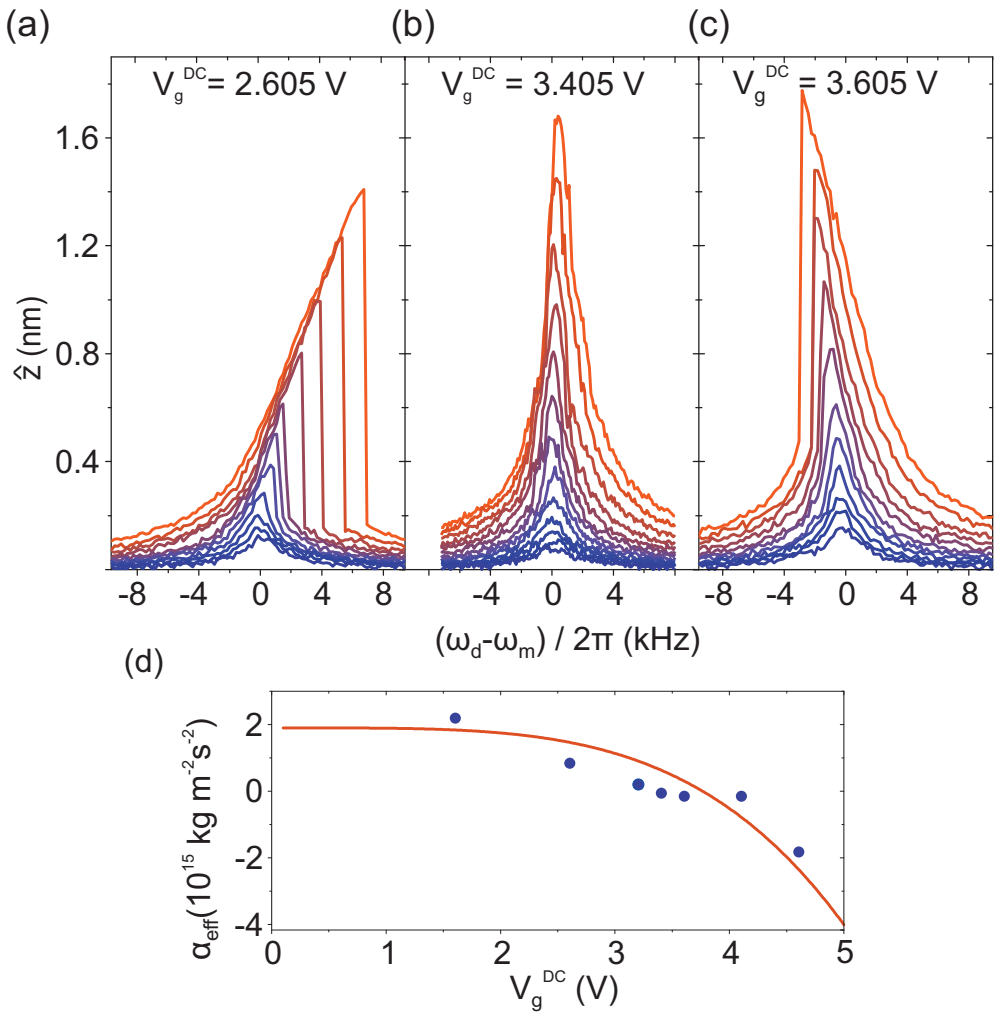

FIG. 5: (a)-(c) Dependence of the vibrational amplitude $\hat{z}$ in device B on the drive frequency for different $V_{\rm g}^{\rm AC}$ in each plots. In (a) and (c), $V_{\rm g}^{\rm AC}$ = 3 μV - 31 μV. In (b) $V_{\rm g}^{\rm AC} = 1.9\mu V - 31\mu V$. The onset of bistability is determined to be at $\hat{z}_{\rm crit}$ = 360 pm for (a) and at $\hat{z}_{\rm crit}$ = 900 pm for (c). (d) Effective Duffing parameter $\alpha_{\rm eff}$ as a function of $V_{\rm g}^{\rm DC}$. The red line is a plot of Eq. (4) with $c_{\rm s} = 0.65$ nm/V^2 and $\alpha_0 = 1.9 \cdot 10^{15}$ kg·m^{-2}s^{-2}.